Thermal Denaturation of *Escherichia coli* Thioredoxin Studied by Hydrogen/Deuterium Exchange and Electrospray Ionization Mass Spectrometry: Monitoring a Two-State Protein Unfolding Transition†

Claudia S. Maier,‡ Michael I. Schimerlik,§ and Max L. Deinzer*,‡

Departments of Chemistry and Biochemistry & Biophysics, Oregon State University, Corvallis, Oregon 97331

Received August 11, 1998; Revised Manuscript Received November 18, 1998

ABSTRACT: Thermally denatured oxidized *Escherichia coli* thioredoxin (TRX) in 2% acetic acid was examined by electrospray ionization mass spectrometry (ESI-MS) and circular dichroism. Conformational dynamics during thermal unfolding were probed by hydrogen/deuterium (H/D) exchange-in experiments. ESI-MS was used to determine the H/D ratios. TRX shows only a marginal change in negative ellipticity at 222 nm during thermal unfolding, but in the near-UV circular dichroism (240−350 nm) a clear transition is observed (T_m = 61 °C), and unfolding goes to completion. ESI mass spectra were recorded as a function of temperature, and the observed bimodal charge state distributions were analyzed assuming a two-state unfolding mechanism which allowed an estimation of the midpoint temperature, T_m = 64 °C. Under conditions at which the compact, folded conformational state is only marginally stable (80 °C, 2% acetic acid-d_1), H/D exchange-in experiments in combination with ESI-MS resulted in mass spectra differing in the number of incorporated deuteriums which indicates the presence of two distinct populations of molecules after short incubation periods. As the exchange-in time increases, the population representing the unfolded state increases and the population which is protected against exchange decreases. The rate of conversion was used to estimate the rate constant of unfolding which was 2.1 ± 0.2 min^{-1}. The results presented here indicate that thermally denatured TRX under the conditions used may represent a collapsed unfolded state with properties often attributed to molten globule-like states, such as pronounced secondary structure but absence of rigid tertiary structure and, hence, lack of protection against H/D exchange.

The stability and dynamics of proteins are often analyzed by examining their unfolding transitions. Most single-domain proteins closely approach a two-state unfolding mechanism, F ⇔ U, where only the folded (F)[1] and unfolded (U) states are populated at equilibrium (*1*). The native state can be unfolded by adding chemical denaturants or by thermal denaturation (*1*, *4*). The most common techniques used to monitor unfolding are DSC (*2*, *3*) and spectroscopic methods, such as CD (*4*), UV absorbance (*5*), and fluorescence (*6*). These techniques measure properties which characterize the ensemble of folded and unfolded states, and thus do not easily distinguish between different populations. H/D exchange is a straightforward approach for measuring unfolding because exchange rates are highly sensitive to changes in surface accessibility and loss of stabilizing hydrogen bonds (*7*, *8*). Approaches in which H/D exchange experiments are combined with nuclear magnetic resonance spectroscopy (*9*−*13*) and mass spectrometry (*14*−*17*) are especially promising. NMR approaches are superior in providing information about the exchange behavior of individual residues. The unique advantage of mass spectrometry is that, besides the determination of the deuterium content, the exchange behavior of coexisting conformations can be distinguished as long as the conformations sampled resulted from individual exchange behavior. The presence of several conformations in equilibrium represents the scenario observed in unfolding experiments in which folded and unfolded states are present simultaneously.

Recently, ESI-MS has been found to be an attractive method which is capable of reflecting conformational changes of proteins in solution (*18*−*24*). During the ESI process, multiply protonated protein ions (charge states) are generated and transferred intact into the gas phase of the mass spectrometer. The observed ESI mass spectra exhibit charge state distributions characteristic of the conformational state in solution which enable one to differentiate between folded, more compact (native) and unfolded, less compact (denatured) states. ESI mass spectra of unfolded, less compact states show higher multiply charged ions than the corresponding folded, more compact forms. At present, only limited experimental evidence is available to fully understand the relationship between observed charge state distributions

† This work was supported in part by the National Institute of Environmental Health Sciences (ES00040 and ES00210), the National Science Foundation (BIR-921 4371), and the Anheuser-Busch Foundation. This is Technical Paper 11451 from the Oregon Agricultural Experiment Station.

* To whom correspondence should be addressed. Phone: (541) 737-1773. Fax: (541) 737-0497. E-mail: deinzerm@ccmail.orst.edu.

‡ Department of Chemistry.

§ Department of Biochemistry & Biophysics.

[1] Abbreviations: 6+, 7+, etc., charge states of a multiply protonated protein molecular ion as observed in ESI-MS experiments; a.u., arbitrary units; CD, circular dichroism; DSC, differential scanning calorimetry; ESI, electrospray ionization; F, folded state; H/D, hydrogen/deuterium; $(M+nD)^{n+}$, *n*-fold deuterated protein ion in the gas phase; $(M+nH)^{n+}$, *n*-fold protonated protein ion in the gas phase; MS, mass spectrometry; *m*/*z*, mass-to-charge ratio; NMR, nuclear magnetic resonance; TRX, *Escherichia coli* thioredoxin; U, unfolded state; UV, ultraviolet.

10.1021/bi981938w CCC: $18.00
Published on Web 12/29/1998

in ESI mass spectra and solution conformations. However, there is general consensus that higher charge states as observed for unfolded, less compact conformations can be explained, at least in part, by the increased steric accessibility of protonation sites accompanied by an eventual change of their pK_a-values and a more extended conformation of the unfolded state (*25*−*28*).

Thioredoxin is a small ubiquitous redox-active protein that has been studied extensively (*29*, *30*). Hiraoki et al. (*31*) investigated the thermal stabilities of oxidized and reduced *E. coli* TRX at pH 7 by proton NMR and CD spectroscopy. The denaturation temperature T_m of oxidized TRX was reported to be 80 °C on the basis of proton NMR data which agreed with the T_m value obtained in the near-UV CD (280 nm). In the far-UV CD (198 nm), the denaturation temperature was found to be roughly 5 °C higher. The thermodynamics of oxidized TRX were also determined by DSC over a pH range of 6−8 (*2*, *3*). These data indicated an inverse dependence of the transition temperature on the protein concentration which was rationalized by a tendency to reversible dimerization of both forms of TRX, the native and denatured one (*2*, *3*).

The present study is an attempt to learn more about the temperature-induced denatured state of oxidized TRX and the conformational dynamics during thermal denaturation by using relatively new techniques capable of monitoring protein conformational properties through H/D exchange in conjunction with ESI-MS experiments. However, ESI mass spectrometric approaches make use of volatile buffer solutions necessary. Hiroaki et al. (*31*) noted that the stability of TRX was unchanged at pH 2.5 and 25 °C, and no signs of denaturation were detected by proton NMR spectroscopy. Consequently, 2% acetic acid was chosen as the solvent system. Low pH and heat possess a synergistic denaturing effect that decreases the transition temperature and, therefore, allowed direct monitoring of the thermal unfolding transition of oxidized TRX by mass spectrometric techniques. This study represents the foundation for future work addressing the influence of protein alkylation by glutathione-activated xenobiotics (*32*) on the stability and structural integrity of TRX.

MATERIALS AND METHODS

Materials. Recombinant oxidized *E. coli* thioredoxin purchased from Calbiochem (La Jolla, CA) was used for mass spectrometric analyses. Recombinant oxidized *E. coli* thioredoxin purchased from Promega (Madison, WI) was used for the spectroscopic analyses. HPLC, CD, and mass spectrometric analysis did not reveal any significant differences between TRX of the two suppliers. Deuterium oxide (99.8%) and acetic acid-d_1 were purchased from Aldrich Chemical Co. (Milwaukee, WI). pH/pD measurements were performed with pHydrion microfine paper from Micro Essential Laboratory (Brooklyn, NY). The d(pK_a)/dT of acetic acid is 0.0002, which is sufficiently low to ensure a constant pH of the protein solution during heat-induced denaturation studies (*33*).

Circular dichroism spectroscopy was performed on a Jasco J720 spectropolarimeter (Jasco Inc., Easton, MD) equipped with a home-built thermoelectrically controlled cell holder. CD spectra of TRX (15.8 μM) were measured in the far-UV range (215−260 nm) in square 1 mm path length quartz cuvettes and with a bandwidth of 2 nm and a scan speed of 10 nm/min. In far-UV CD experiments, the temperature was measured with a thermocouple element glued to the outside of the cuvette wall. Equilibrium thermal denaturation of TRX in 2% acetic acid-d_1 (pH 2.8−3.1) was monitored at 222 nm. The temperature was manually increased from 25 to 75 °C. Equilibration time at each temperature point was 15 min, and signal averaging time was 4 min.

Near-UV CD experiments were carried out in cylindrical 1 cm path length quartz cuvettes. The protein concentration was 36.7 μM. The temperature probe was immersed into the protein solution during heat denaturation experiments. The temperature was manually increased from 25 to 75 °C; the equilibration time at each temperature step was 15 min. CD spectra were obtained by averaging three spectra obtained with a bandwidth of 2 nm and a scan speed of 10 nm/min over a wavelength range of 240−360 nm. All spectra were smoothed with software provided with the instrument and base line-corrected for the CD signal in the absence of protein. Reversibility of thermal denaturation was checked by stepwise cooling of the protein solution after acquiring its CD spectrum at the maximum denaturation temperature. As judged by the ellipticity at 280 nm, the reversibility was better than 85%.

The mean residue molar ellipticity $(\theta)_\lambda$ at a given wavelength was calculated according to eq 1:

$$(\theta)_\lambda \text{ (deg cm}^2 \text{ dmol}^{-1}) = [(\text{MW}/n)\theta_\lambda]/(100[\text{P}]l) \quad (1)$$

where θ_λ is the observed ellipticity in degrees, MW is the molecular weight of oxidized TRX (11 674), n is the number of residues (n = 108), [P] is the protein concentration in mol dm^{-3}, and l is the path length in centimeters.

Data analyses of equilibrium thermal unfolding experiments were performed assuming a two-state unfolding mechanism and correcting for sloping of the folded and unfolded baselines. Data were fit to eq 2 using Jandel Scientific SigmaPlot 3.0 software:

$$y = b_f + m_f T + (b_u + m_u T)\frac{\exp[(-\Delta H_m(1 - T/T_m))/RT]}{1 + \exp[(-\Delta H_m(1 - T/T_m))/RT]} \quad (2)$$

where y represents the observed CD signal, b_f and b_u are the intercepts, m_f and m_u represent the slopes of the pre-and post-transition base lines, T is the temperature (in degrees kelvin), T_m is the midpoint transition temperature, and ΔH_m is the enthalpy change for unfolding at T_m (*34*). The relative error of the thermodynamic parameter obtained is estimated to be approximately 5−10% and is mainly caused by the manually performed temperature control.

Protein concentrations were determined by UV spectroscopy. An extinction coefficient of 13 700 M^{-1} cm^{-1} at 280 nm for oxidized TRX was used (*35*).

ESI-MS measurements were performed on a PE-Sciex API III triple quadrupole mass spectrometer (PE-Sciex Instruments, Thornhill, Ontario) equipped with a nebulizer-assisted electrospray source. The ion spray needle was maintained at 5300 V. An orifice voltage of 80 V was used for all measurements. A continuous flow setup with loop injection was used for sample infusion and a syringe pump (Model

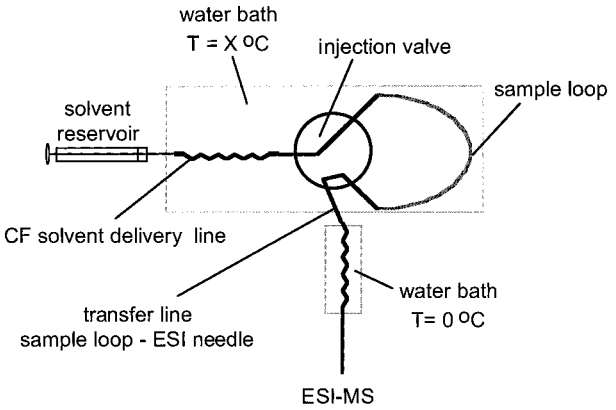

FIGURE 1: Instrumentation used for the H/D exchange-in experiments monitored online by ESI-MS.

11, Havard Apparatus, South Natik, MA) for solvent delivery. For acquiring temperature-dependent ESI mass spectra, the protein solution (0.009 mM in 2% acetic acid, pH 2.8−3.1) was injected into the sample loop of a Rheodyne injection valve (Model 8125), maintained at the desired temperature. The protein solution was equilibrated at the desired temperature for 10 min and then directly infused with a flow rate of 0.005 mL/min via a fused silica capillary (i.d. 0.075 mm, 15 cm) into the electrospray source.

When online H/D exchange/ESI-MS experiments were performed, the solvent delivery line, the sample loop, and the injection valve were immersed in a water bath and equilibrated at the desired temperature. The sample loop (peek tubing i.d. 0.010 in., o.d. 1/16 in., 65 cm) was used as a reaction capillary. The protein solution was transferred into the ESI source via a fused silica capillary (i.d. 0.075 mm, 100 cm) which was immersed in ice water to quench exchange-in and to facilitate refolding of thermally unfolded TRX (Figure 1). The time necessary for the transport of the protein from the sample loop to the ESI needle was approximately 57 ± 3 s at a flow rate of 0.005 mL/min. The incubation periods reported represent the time that the protein sample spent in the sample loop. No efforts were made to minimize back-exchange of deuterium labels during the ESI process.

H/D exchange was initiated by 100-fold dilution of a 0.85 mM TRX stock solution in 2% acetic acid into ice-cold 2% acetic acid-d_1 which resulted in a final protein concentration of 0.009 mM. The protein solution was injected as quickly as possible into the sample loop (approximately 15−20 s). To minimize exchange during this period, the glass body of the syringe was precooled prior to injection.

The *m*/*z*-values for the observed ion peaks represent centroids. The average masses for the protein sample were calculated from the 7-, 8-, and 9-fold charged molecular ion after minimal smoothing. The unfolding rate constant k_1 was estimated by fitting the intensity of the 8-fold charged ion peak at the lower *m*/*z*-value (F) divided by the sum of the intensity of the ion peak at the lower *m*/*z*-value (F) and the intensity of the ion peak at the higher *m*/*z*-value (U) versus time (t) to the expression $F/(F + U) = a \exp(-k_1 t)$.

Analyses of heat-induced changes of bimodal charge state distributions were performed by assuming that the compact conformational state of TRX encompasses the charge states 6+ to 9+ (designated F) and the disordered, denatured conformational states the charge states 10+ to 15+ (designated U). The thermal unfolding curve as a function of temperature was obtained by calculating the ion peak intensity ratio $I_F/(I_F + I_U)$, where I_F and I_u were obtained by summing the ion peak intensities of charge states assigned to the compact conformational state (F) and the disordered, denatured state (U), respectively (*19*). Data analyses were performed according to eq 2 with y as ion peak intensity ratio $I_F/(I_F + I_U)$.

An alternative approach for analyzing charge state distributions observed in ESI-MS experiments was reported by Konermann et al. (*20*). It is based on the calculation of the average charge state $\langle c \rangle$ of an ESI mass spectrum, whereby c denotes the charge state of an ion peak and I_c its intensity (counts per second):

$$\langle c \rangle = \frac{\sum_c I_c c}{\sum_c I_c} \tag{3}$$

Because of inaccuracies of temperature settings/measurements in the high-temperature range (T > 60 °C), inevitable intensity fluctuations of the ion peak signals during the ESI analysis, and uncertainties in the contributions of the $(M+9H)^{9+}$ ion peak to U or F states, the relative error of the thermodynamic data obtained from the analyses of charge state distributions was estimated to be in the range of 10−20%.

RESULTS

Probing the Thermally Induced Conformational Dynamics of TRX by H/D Exchange Experiments Monitored by ESI-MS. Oxidized *E. coli* TRX contains 108 amino acid residues. The number of exchangeable hydrogens is 173 (102 backbone amide hydrogens, 68 side chain hydrogens, and 3 hydrogens from N- and C-termini). In H/D exchange-in experiments, protein conformers with reduced hydrogen bonding and/or increased solvent accessibility show higher deuterium incorporation than do the more compact conformers. In the present design, the progress of deuterium uptake is monitored online by ESI-MS. Thus, multiply deuterated ions $(M+nD)^{n+}$ are observed rather than multiply protonated species $(M+nH)^{n+}$. Deuterium incorporation in proteins can be expressed as the percentage mass increase relative to the maximum number of exchangeable hydrogens. Two reference points were established. The first reference point was obtained by online H/D-exchange analysis of TRX under conditions at which the native state is stable. Under these conditions (2% acetic acid-d_1 at 20 °C), the molecular mass increases of about 30 ± 3Da (17 ± 2%) and 62 ± 5 Da (36 ± 3%) were observed after an incubation period of 4s (the earliest time point possible after injection) and 10 min (the longest time possible after injection), respectively. For the second reference point, TRX was incubated for 2.5 h at 70 ± 5 °C in 2% acetic acid-d_1 which established the highest observable deuterium incorporation. The mass analysis yielded a molecular mass of 11 805 ± 4 Da, indicating an increase of 130 ± 4 Da (75 ± 2%). This sample is referred to as fully deuterated TRX.

The conformational dynamics of TRX during thermal denaturation were investigated by performing online H/D

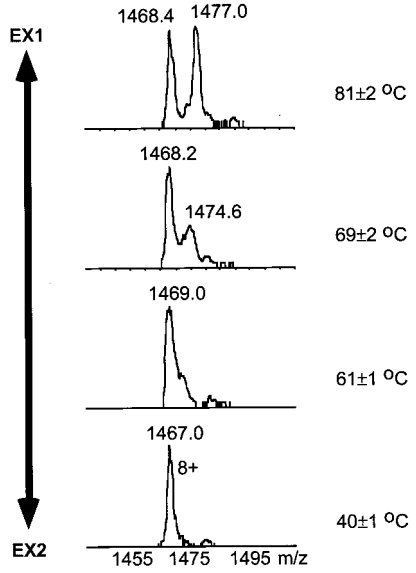

FIGURE 2: Temperature-dependent alteration of the exchange mechanism. Comparison of the 8-fold charged ion peak of *E. coli* thioredoxin at different temperatures after an exchange-in period of 28 ± 4 s in 2% acetic acid-d_1.

exchange-in experiments as a function of temperature and time. In the present experimental design, the thermal denaturation and H/D exchange-in reactions were performed in a capillary assembled in a conventional injection valve and directly connected to the infusion capillary of the ESI source. Refolding of the protein and quenching of the H/D exchange reactions were initiated by rapid cooling of the protein solution. This continuous flow design allowed the direct monitoring of the unfolding transition by ESI-MS. In these experiments, charge states 7+ to 9+ were monitored which were ascribed to the compact conformational state of TRX. Because the 8-fold charged ion peak showed the highest intensity, this charge state of TRX was used to compare the observed ion peaks after an exchange-in period of 28 ± 4 s (Figure 2). During the online exchange-in experiment at 40 °C, the 8-fold charged ion peak was binomial, and the *m*/*z*-value increased to *m*/*z* 1468.6 after 6.3 min which indicated an incorporation of roughly 62 ± 6 deuteriums (36 ± 3%). As the exchange-in was monitored at approximately 60 °C, the ion peaks became broader. A further experiment performed at 65 °C revealed that each ion peak split into two distinct peaks after a brief incubation period. Exchange-in experiments above 65 °C showed the same result. For example, at approximately 80 °C an ion peak appeared at *m*/*z* 1477.2 in addition to the peak at *m*/*z* 1468.4. The ion peak at lower *m*/*z*-value corresponds closely to the ion peak which was observed during the hydrogen exchange experiment under nondenaturing conditions (40 °C), and the peak at the higher *m*/*z*-value was very close to the *m*/*z*-value that was observed for the ion of fully deuterated TRX. The observed mass increment corresponded to an incorporation of 68 ± 6 deuteriums. As the exchange-in time increased, the ion peak at the higher *m*/*z*-value increased in intensity, and the ion peak at the lower *m*/*z*-value diminished (Figure 3).

Equilibrium Thermal Denaturation of TRX Studied by ESI-MS. Continuous flow ESI-MS was used to follow heat-induced conformational changes. The 8.5 μM TRX solution in 2% acetic acid (pH 2.8−3.1) was equilibrated at the

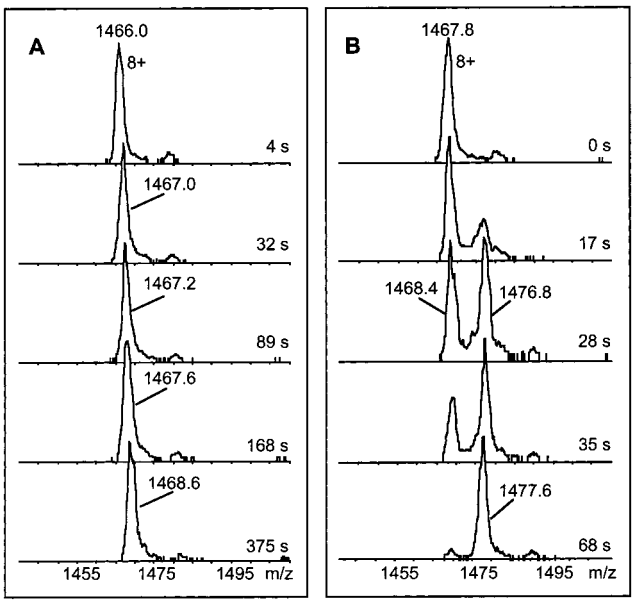

FIGURE 3: Evolution of the 8-fold charged ion peak of *E. coli* thioredoxin during the online H/D exchange-in experiments in 2% acetic acid-d_1 at 40 °C (A) and at 80 °C (B). The time points given refer to incubation periods.

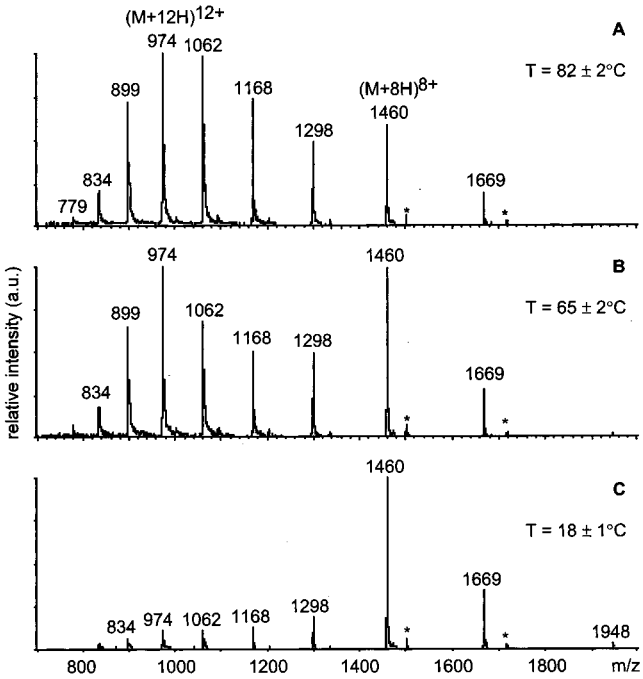

FIGURE 4: ESI mass spectra of *E. coli* thioredoxin in 2% acetic acid at different temperatures: (A) 82 ± 2 °C, (B) 65 ± 2 °C, and (C) 18 ± 1 °C. Ion peaks at *m*/*z* 1948, 1669, 1460, and 1298 representing charge states 6+, 7+, 8+, and 9+, respectively, were attributed to the folded form F. Ion peaks at *m*/*z* 1168, 1062, 974, 899, 834, and 779 representing charge states 10+ to 15+ were ascribed to the charge state distribution which was assumed to have originated from the unfolded form U. A minor unidentified impurity is marked with an asterisk.

desired temperature in the sample loop of the injection valve and directly infused into the ESI-MS source. Under the conditions used, TRX showed ESI mass spectra (Figure 4) which were characterized by a narrow charge state distribution at higher *m*/*z*-values encompassing the 6- to 9-fold protonated ions with the $(M+8H)^{8+}$ ion as the dominant ion peak. In the lower *m*/*z* range, a second set of peaks with

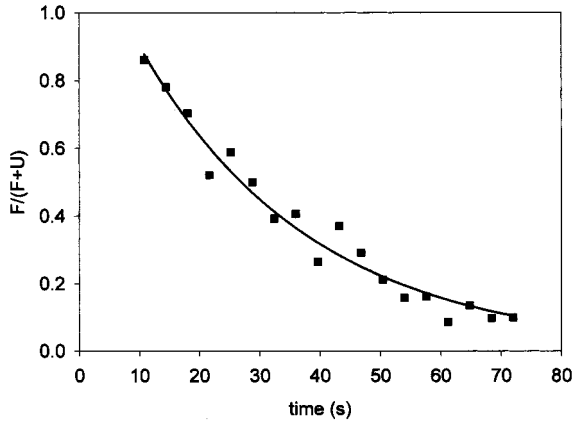

FIGURE 5: Estimation of the rate constant k_1 for unfolding. The continuous line is a theoretical curve based on the expression $F/(F + U) = a \exp(-k_1 t)$, whereby the ion peak intensity ratio $F/(F + U)$ was derived from the time course of conversion of the ion peak at *m*/*z* 1467.8 (*F*) to *m*/*z* 1477.6 (*U*) as illustrated in Figure 3B.

low intensity was observed which encompassed the 10- to 15-fold protonated charge states with $(M+12H)^{12+}$ being the most abundant ion. The distribution of the charge states significantly changed as the temperature of the protein solution was increased above 40 °C. The relative intensity of the 6- to 8-fold protonated ions decreased, and the intensity of the 9- to 15-fold protonated ions increased. As the temperature approached 65 °C, the $(M+8H)^{8+}$ and $(M+12H)^{12+}$ ion peaks became equally intense. Further increase in temperature led to domination of the ion peaks at lower *m*/*z*-values representing the charge states 10+ to 15+.

Equilibrium Thermal Denaturation Probed by CD Spectroscopy. Far-UV CD was used to examine changes in the secondary structure of TRX during thermal denaturation. The far-UV CD spectrum of TRX (in 2% acetic acid-d_1 and 25 °C) showed a broad negative minimum at 218−222 nm. The absence of two distinct negative minima at approximately 208 and 222 nm classified TRX (under the conditions used) as an α/β class protein (*36*). By increasing the temperature to 75 °C, only a small change in negative ellipticity at 222 nm was observed (Figure 6A).

This is in contrast to the clear transition observed in near-UV CD during thermal denaturation of TRX in 2% acetic acid-d_1 (Figure 6B). Changes in the near-UV CD reflect changes in the environment of aromatic amino acid residues. TRX possesses two tryptophan, two tyrosine, and four phenylalanine residues which in the rigid tertiary structure are responsible for a pronounced maximum at 280 nm. Increasing the temperature caused a decrease in the CD signal which reached its lower limits above 70 °C.

DISCUSSION

Conformational Dynamics of TRX during Heat Denaturation. Thermally induced unfolding of small proteins can often be described by a two-state transition model in which the folded state is represented as a relatively narrow distribution of highly structured conformations stabilized by hydrogen bonding, and the unfolded state as a heterogeneous distribution of less compact conformations lacking significant hydrogen bonding (*37*). Protection against hydrogen exchange is dramatically enhanced in the presence of hydrogen bonding; i.e., in a structured protein, exchange rates are

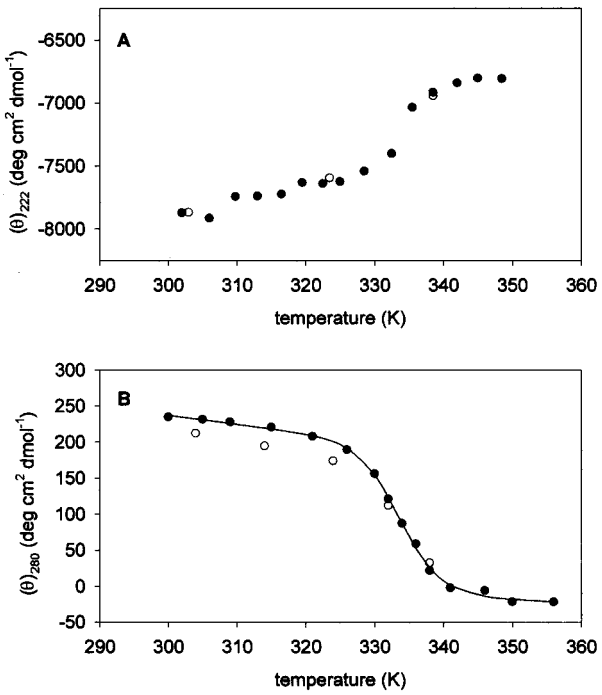

FIGURE 6: Far-UV (A) and near-UV (B) CD heat denaturation curve of *E. coli* thioredoxin in 2% acetic acid-d_1. The mean residue molar ellipticity $(\theta)_\lambda$ is given in deg cm^2 dmol^{-1} during the heating (●) and cooling (○) phases of the unfolding experiments. (A) Note the only marginal change of the far-UV CD signal at 222 nm during thermal denaturation. (B) The continuous line is a theoretical curve based on eq 2.

retarded by a factor of 10^6-10^8 compared to the rates observed in random coil like peptides. Hydrogen exchange on proteins can be approximated by the following model (*7*, *38*):

$$F_H \underset{k_{-1}}{\overset{k_1}{\rightleftharpoons}} U_H \xrightarrow{k_2} U_D \underset{k_{-1}}{\overset{k_1}{\rightleftharpoons}} F_D$$

$$k_{ex} = \frac{k_2 k_1}{k_{-1} + k_2}$$

Two rate-limiting processes can be considered to correlate protein unfolding with the experimental data. If interconversion between the closed (F) and open (U) structures is much faster than the intrinsic chemical exchange rate, i.e., $k_2 \ll k_{-1}$, opening and refolding will occur many times before exchange takes place. Under conditions favoring the native state, local refolding can occur in less than a microsecond and even global unfolding reactions may take place within 50 ms (*8*). This exchange mechanism is termed EX2, and $k_{ex} = k_2(k_1/k_{-1})$. Under denaturing conditions, however, the native state is only marginally stable, and interconversion between the open (U) and closed (F) structures is slow compared to the chemical exchange rate, i.e., $k_2 \gg k_{-1}$. If the rate-limiting step is determined by k_{-1}, exchange occurs by an EX1 mechanism, and the experimentally observed exchange rate constant k_{ex} is directly related to the unfolding rate constant k_1 ($k_{ex} = k_1$). Mass spectrometric approaches to monitor exchange reactions can be used to distinguish between these exchange mechanisms (*15*, *17*). When H/D exchange occurs by the EX2 mechanism, the mass spectrum shows a peak that shifts with increasing exchange-in time

to higher masses. In contrast, two distinct mass peaks develop after a short exchange-in time if exchange occurs via the EX1-type mechanism. The mass peak at higher masses represents the molecules that experienced global unfolding. Hence, these molecules spent enough time in the unfolded state to allow their core amide protons to exchange with deuteriums. The mass peak at lower masses originated from the population of molecules that did not unfold at the time point of sampling and, therefore, shows lower deuterium incorporations because their core amide protons are still protected against exchange-in. The difference in deuterium incorporation between these two populations is observed in the mass spectrum as a mass shift. If H/D exchange occurs via an EX1-type reaction, mass spectrometric-based approaches allow an estimate of the unfolding rate constant k_1 which can be obtained from the rate of conversion of the mass peak at the lower *m*/*z*-value and the peak at the higher *m*/*z*-value (*15*, *39*).

A single mass peak which moves gradually to higher masses over time at $T < 40$ °C indicates that the folded conformer is stable under the applied conditions and exchange occurs via an EX2 mechanism (Figure 3A). Many opening and closing reactions occur prior to a successful exchange event. Hence, each molecule experiences an average number of successful exchanges. The observed peak width at half-height is relatively narrow over the entire exchange-in time period sampled, suggesting that the distribution of conformers probed is relatively small, and that exchange occurs by local unfolding. However, it should be noted that subglobal or even global unfolding reactions may occur in less than 50 ms (*8*).

As the incubation temperature is increased, a broadening of the ion peaks is observed, indicating that the number of conformations with individual exchange behavior is increased. The splitting into two distinct ion peaks at approximately 61 °C marks the melting of the native protein conformer. Above the melting temperature, two well-separated ion peaks are observed, indicating the change to an exchange mechanism under which global unfolding reactions dominate and the native state is only marginally stable. Under EX1 conditions, a protein spends sufficient time in the unfolded or unprotected state so that almost all of the exposed protons are exchanged. This gives rise to two populations of molecules in solution: those molecules that have undergone a global unfolding and those that have not, in which case their core amide hydrogens are still protected against exchange. As the exchange-in time increases, the population representing the unfolded state increases and the population protected against exchange decreases (Figure 3B).

The rate of conversion of the 8-fold charged ion peak at lower *m*/*z*-value to the ion peak at higher *m*/*z*-value was used to estimate the rate constant for unfolding, k_1, to be 2.1 ± 0.2 min^{-1} (Figure 5). The amide proton exchange rates in a random coil with the sequence of oxidized TRX at 82 °C (355 K) and at pD 2.8 are predicted to range from 1.2 to 180 min^{-1} (*40*). The *m*/*z*-value of the lower ion peak as well as the ion peak at higher *m*/*z*-value increased slowly, and a concomitant narrowing of the ion peak at higher *m*/*z*-value was observed during the exchange course which indicates that exchange does not occur exclusively by an EX1 mechanism. In this context, it should be noted that 29 backbone amide hydrogens (of 102 possible) possess intrinsic exchange rate constants k_2 in the range of 1.2−5.6 min^{-1} (*40*), i.e., of the same magnitude as the estimated unfolding rate k_1. Although small variations in the masses and peak widths at half-height were observed during the course of the exchange at 80 °C, the evolution of two distinct mass peaks allows the conclusion that, under the conditions applied, the breaking of the intramolecular hydrogen bonds may be described as a cooperative two-state process (*15*).

Equilibrium Thermally Induced Denaturation Studied by CD and ESI-MS. The sharp transition observed in near-UV CD during heat-induced denaturation of TRX in 2% acetic acid-d_1 monitored the thermally induced loosening of tightly packed aromatic side chains and consequent collapse of the tertiary structure of TRX (Figure 6). Assuming that the observed transition can be approximated by a two-state unfolding mechanism in which only the folded and unfolded forms are significantly populated, the melting temperature T_m (midpoint of transition) was estimated to be 60 °C (333 K) and the enthalpy change for unfolding ΔH_m 78 kcal/mol. However, the observed negative ellipticity in the far-UV CD suggests a high content of secondary structure remaining in thermally denatured TRX (Figure 6A). Similar discrepancies between the near-UV and far-UV CD experiments have been reported for other thermally denatured proteins, including ribonuclease A (*9*), α-chymotrypsinogen (*41*), bovine α-lactalbumin (*42*) and several pore-forming toxins, e.g., diphtheria toxin (*43*) or equinatoxin II (*44*).

ESI-MS is emerging as a technique that is potentially sensitive to conformational changes of proteins in solution. Thus, ESI mass spectra of denatured proteins show charge state distributions with higher degrees of protonation than intact, native proteins electrosprayed under the same conditions (*18*, *19*, *21*, *24*−*27*, *45*). The influence of mutations on the global stability of bacterial cytochrome *c* was evident through alterations in charge state distributions (*46*). Recently, Konermann et al. showed that the changes of charge state distributions can be applied to monitor protein folding of cytochrome *c* (*23*) and acid-induced unfolding of myoglobin (*22*) when studied by time-resolved ESI-MS.

TRX shows temperature-dependent charge state distributions in ESI-MS experiments under the conditions described here (Figure 4). The charge state distribution at higher *m*/*z*-values centered around the 8-fold protonated ion peak is attributed to compact, tightly folded conformational states of TRX, whereas the charge state distribution at lower *m*/*z*-values centered around the 12-fold protonated ion peak originates from loosely packed or unfolded conformational states. At all temperatures studied, TRX showed only these two distributions, and these undergo temperature-dependent changes in intensity without shifting of their maxima. The lack of intermediate charge state distributions which would indicate the formation of partially folded conformational states during equilibrium thermal denaturation experiments justifies the interpretation that thermal unfolding of TRX under the conditions used essentially involves a two-state system: a folded form (F) and an unfolded form (U). Thus, the ion peak intensities reflect the proportion of folded or unfolded molecules, respectively. Analysis of the heat denaturation curve according to eq 2 yielded $T_m = 64$ °C (337 K) and an estimated $\Delta H_m = 74$ kcal/mol for thermal unfolding of TRX in 2% acetic acid (pH 2.8−3.1) (Figure 7). Additionally, analysis of the temperature-dependent

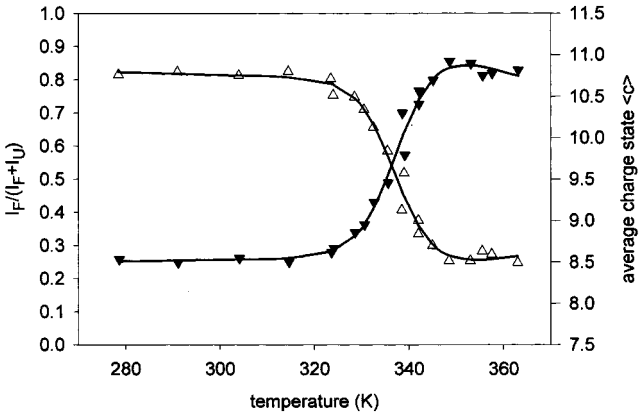

FIGURE 7: Heat denaturation curves of *E. coli* thioredoxin in 2% acetic acid deduced from the temperature-dependent charge state distributions obtained by ESI-MS: (△) ion peak intensity ratio; (▼) average charge state ⟨*c*⟩ as a function of temperature. The continuous lines are theoretical curves based on eq 2.

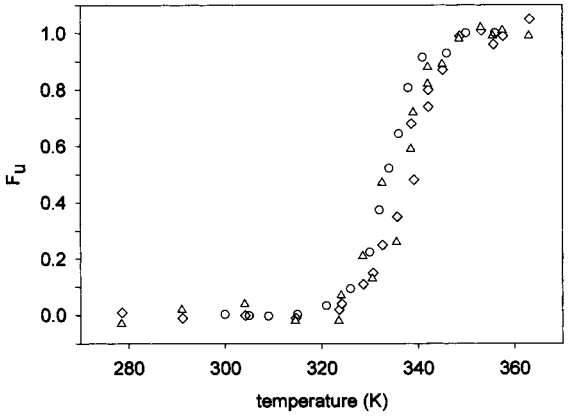

FIGURE 8: Fraction unfolded versus temperature curves were generated from data presented in Figure 6B and Figure 7: (○) near-UV CD signal at 280 nm; (△) ion peak intensity ratio; (◇) average charge state ⟨*c*⟩ .

charge state distributions was performed according to eq 3 (*20*) and yielded the average charge state ⟨*c*⟩ of each ESI mass spectrum as a function of temperature (Figure 7). Again, a distinct unfolding transition was obtained which allowed the estimation of T_m and ΔH_m according to a two-state model as 65 °C (338 K) and 54 kcal/mol, respectively.

In this respect, ESI charge state distributions may provide a more direct method to estimate the fraction of folded and unfolded molecules than optical spectroscopic methods which usually measure the sum of signals of both forms, folded and unfolded. At the present time, there is still only limited knowledge available on how charge states and ion peak intensities in ESI-MS are influenced during ion evaporation in the electrospray ionization process (*25*, *28*, *47*). However, work on the acid-mediated unfolding of cytochrome *c* recently published by Konermann et al. (*20*) demonstrated that analyses of charge state distributions generated by ESI-MS yielded results that agreed well with those obtained by optical spectroscopy.

In the present study, the temperature-dependent unfolding transition determined by analysis of the charge state distributions in the ESI mass spectra coincided with the unfolding transition observed in the near-UV CD that reflected the collapse of the tertiary structure (Figure 8). The H/D-exchange experiments indicate that the alteration of the exchange mechanism from EX2 to EX1 occurred roughly in the same temperature range. This suggests that charge state distributions observed in ESI-MS reflect on the intactness of the hydrogen bonding network and, therefore, may actually represent a sensitive technique capable of monitoring subtle changes in the entirety of the tertiary structure. Similar conclusions were reached by Pan et al. (*48*) during a study of the acid-induced conformational changes of RNase A and by Konermann et al. (*20*, *21*) on the pH-dependent unfolding studies of cytochrome *c*.

An important structural feature of oxidized TRX is its hydrophobic core consisting of a five-stranded twisted β-sheet surrounded by four α-helices and a 3_{10} helix (*49*) which causes the surprisingly high stability against thermal denaturation (*35*). To study the thermal denaturation dynamics, acidic conditions were chosen which destabilized the native conformational state and ensured that the unfolding transition could be monitored. TRX showed a minor decrease of ellipticity in the near-UV CD in 2% acetic acid-d_1 as compared to the ellipticity obtained in phosphate buffer (pH 6.8), which may indicate that some minor structural disturbance occurred. However, the exchange-in experiments at ambient temperature demonstrated that under the conditions used, TRX possesses a stable rigid tertiary structure which is in agreement with previous NMR data (*31*). The gradual recovery of the ellipticity at 280 nm indicated that the thermal denaturation was reversible to a large extent and that the asymmetric environment of the aromatic chromophores, and thus the overall structural integrity, was reestablished during cooling (Figure 6). Based on DSC studies, Ladbury et al. (*2*, *3*) reported that TRX may have some tendency to form dimers and/or oligomers. The protein concentrations used in the mass spectrometric experiments described here were significantly lower (in the lower micromolar range) than those used in the DSC experiments which were in the millimolar range (*2*, *3*). Furthermore, at acid pH, solvent-exposed residues are protonated. This may tend to suppress dimerization by charge repulsion.

The nature of the chiral structure measured in the far-UV CD (222 nm) of thermally denatured TRX must still be addressed. Thermal unfolding in conjunction with H/D exchange experiments showed: (a) the evolution of two distinct mass peaks representing compact and unfolded populations, respectively, that indicated cooperative breaking of the hydrogen bonding network and (b) the absence of any significantly populated intermediate states during thermal unfolding. Furthermore, the evolution of a mass peak during the exchange-in experiment corresponding to fully deuterated TRX proved that there was at best only weak protection against deuterium exchange-in in thermally unfolded TRX. The absence of ellipticity in the near-UV CD of thermally denatured TRX suggested the absence of tightly packed aromatic side chains and, therefore, the absense of a rigid tertiary structure. However, the negative ellipticity detected by far-UV CD indicated the presence of secondary structure. These observations support the conclusion that thermally denatured TRX can be described as a thermodynamically stable intermediate with properties associated with molten globule-like states (*50*−*52*). By applying Baldwin's classification of molten globule-like states (*51*), the term collapsed unfolded state to describe thermally unfolded TRX is preferred over molten globule. Structural descriptions of

collapsed unfolded states are still emerging. However, models have been proposed in which hydrophobic patches promote the formation of some kind of transient secondary structural elements throughout the collapsed protein (*53*). The transient nature of these interactions would at least partially explain the presence of some kind of average chiral structure detected by far-UV CD and the simultaneous lack of protection against amide proton exchange. The H/D exchange experiments did not directly address the question whether any specific native-like structural elements remain in thermally denatured TRX that would classify the observed state as a true molten globule. Spectroscopic methods that use different structural probes may even reveal more complex processes. Recently reported work on a disulfide-shuffled, three disulfide-containing bovine α-apolactalbumin (*16*) and the A-state of cytochrome *c* (*54*) demonstrated that true molten globules experience exchange-in kinetics which are between those of the native and the unfolded states. Hence, the observed exchange behavior according to an EX1 mechanism without significantly populated intermediate states supports the classification of thermally denatured TRX as a collapsed unfolded form.

ACKNOWLEDGMENT

We thank Dr. W. C. Johnson, Jr. for helpful discussions and access to his CD instrument. We also thank D. A. Griffin and J. Lawrence for technical assistance. We are grateful to Dr. A. D. Robertson, University of Iowa, for allowing us to use his spreadsheet for the calculation of the intrinsic exchange rate constants.

REFERENCES

1. Creighton, T. E. (1990) *Biochem. J. 270*, 1−16.
2. Ladbury, J. E., Wynn, R., Hellinga, H. W., and Sturtevant, J. M. (1993) *Biochemistry 32*, 7526−7530.
3. Ladbury, J. E., Wynn, R., Thomson, J. A., and Sturtevant, J. M. (1995) *Biochemistry 34*, 2148−2152.
4. Swint, L., and Robertson, A. D. (1993) *Protein Sci. 2*, 2037−2049.
5. Thomson, J. A., Shirley, B. A., Grimsley, G. R., and Pace, C. N. (1988) *J. Biol. Chem. 264*, 11614−11620.
6. Eftink, M. R. (1994) *Biophys. J. 66*, 482−501.
7. Englander, S. W., and Kallenbach, N. (1984) *Q. Rev. Biophys. 16*, 521−655.
8. Englander, S. W., Sosnick, T. R., Englander, J. J., and Mayne, L. (1996) *Curr. Opin. Struct. Biol. 6*, 18−23.
9. Robertson, A. D., and Baldwin, R. L. (1991) *Biochemistry 30*, 9907−9914.
10. Bai, Y., Milne, J. S., Mayne, L., and Englander, S. W. (1994) *Proteins: Struct., Funct., Genet. 20*, 4−14.
11. Bai, Y., Sosnick, T. R., Mayne, L., and Englander, S. W. (1995) *Science 269*, 192−197.
12. Bai, Y., and Englander, S. W. (1996) *Proteins: Struct., Funct., Genet. 24*, 145−151.
13. Radford, S. E., Buck, M., Topping, K. D., Dobson, C. M., Evans, P. A. (1992) *Proteins: Struct., Funct., Genet. 14*, 237−248.
14. Smith, D. L. (1998) *Biochemistry 63*, 285−293.
15. Yi, Q., and Baker, D. (1996) *Protein Sci. 5*, 1060−1066.
16. Robinson, C. V., Gross, M., Eyles, S. J., Ewbank, J. J., Mayhew, M., Hartl, F. U., Dobson, C. M., and Radford, S. E. (1994) *Nature 372*, 646−372.
17. Miranker, A., Robinson, C. V., Radford, S. E., Aplin, R. T., and Dobson, C. M. (1993) *Science 262*, 896−899.
18. Chowdhury, S. K., Katta, V., and Chait, B. T. (1990) *J. Am. Chem. Soc. 112*, 9012−9013.
19. Mirza, U. A., Cohen, S. L., and Chait, B. T. (1993) *Anal. Chem. 65*, 1−6.
20. Konermann, L., and Douglas, D. J. (1997) *Biochemistry 36*, 12296−12302.
21. Konermann, L., and Douglas, D. J. (1998) *Rapid Commun. Mass Spectrom. 12*, 435−442.
22. Konermann, L., Rosell, F. I., Mauk, A. G., and Douglas, D. J. (1997) *Biochemistry 36*, 6448−6454.
23. Konermann, L., Collings, B. A., and Douglas, D. J. (1997) *Biochemistry 36*, 5554−5559.
24. Przybylski, M., and Glocker, M. O. (1996) *Angew. Chem., Int. Ed. Engl. 35*, 806−826.
25. Le Blanc, J. C. Y., Beuchemin, D., Siu, K. W. M., Guevremont, R., and Berman, S. S. (1991) *Org. Mass Spectrom. 26*, 831−839.
26. Loo, J. A., Ogorzalek, R. R., Udseth, H. R., Edmonds, C. G., and Smith, R. D. (1991) *Rapid Commun. Mass Spectrom. 5*, 101−105.
27. Katta, V., and Chait, B. T. (1991) *Rapid Commun. Mass Spectrom. 5*, 214−217.
28. Fenn, J. B. (1993) *J. Am. Soc. Mass Spectrom. 4*, 524−535.
29. Holmgren, A. (1985) *Annu. Rev. Biochem. 54*, 237−271.
30. Holmgren, A. (1989) *J. Biol. Chem. 264*, 13963−13966.
31. Hiraoki, T., Brown, S. B., Stevenson, K. J., and Vogel, H. J. (1988) *Biochemistry 27*, 5000−5008.
32. Erve, J. C., Barofsky, E., Barofsky, D. F., Deinzer, M. L., and Reed, D. J. (1995) *Chem. Res. Toxicol. 8*, 934−941.
33. Stevens, L. (1996) in *Proteins* (Price, N. C., Ed.) pp 21−26, Bios Scientific Publishers Lim, Oxford, U.K.
34. Santoro, M. M., and Bolen, D. W. (1988) *Biochemistry 27*, 8063−8068.
35. Reutimann, H., Straub, B., Luisi, P. L., and Holmgren, A. (1981) *J. Biol. Chem. 256*, 6796−6803.
36. Manavalan, P., and Johnson, W. C., Jr. (1983) *Nature 305*, 831−832.
37. Creighton, T. E. (1990) *Biochem. J. 270*, 1−16.
38. Clarke, J., Itzhaki, L. S., and Fersht, A. R. (1997) *Trends Biochem. Sci. 22*, 284−287.
39. Zhang, Z., Li, W., Li, M., Logan, T. M., Guan, S., and Marshall, A. G. (1997) in *Techniques in Protein Chemistry VIII* (Marshak, D. R., Ed.) pp 703−713, Academic Press, San Diego, CA
40. Bai, Y., Milne, J. S., Mayne, L., and Englander, S. W. (1993) *Proteins: Struct., Funct., Genet. 17*, 75−86.
41. Chalikian, T. V., Völker, J., Anai, D., and Breslauer, K. J. (1997) *J. Mol. Biol. 274*, 237−252.
42. Kuwajima, K. (1985) *Biochemistry 24*, 874−881.
43. Zhao, J. M., and London, E. (1986) *Proc. Natl. Acad. Sci. U.S.A. 83*, 2002−2006.
44. Poklar, N., Lah, J., Salobir, M., Maček, P., and Vesnaver, G. (1997) *Biochemistry 36*, 14345−14352.
45. Loo, J. A., Edmonds, C. G., Udseth, H. R., and Smith, R. D. (1990) *Anal. Chem. 62*, 693−698.
46. Rémigy, H., Jaquinod, M., Pétillot, Y., Gagnon, J., Cheng, H., Xia, B., Markley, J. L., Hurley J. K., Tollin, G., and Forest, E. (1997) *J. Protein Chem. 16*, 527−532.
47. van Berkel, G. J., and Zhou, F. (1995) *Anal. Chem. 67*, 2916−2923.
48. Pan, X. M., Sheng, X. R., Yang, S. M., and Zhou, J. M. (1997) *FEBS Lett. 402*, 25−27.
49. Katti, S. K., LeMaster, D. M., and Eklund, H. (1990) *J. Mol. Biol. 212*, 167−184.
50. Chaffotte, A., Guijarro, J. I., Guillou, Y., Delepierre, M., and Goldberg, M. E. (1997) *J. Protein Chem. 16*, 433−439.
51. Baldwin, R. L. (1991) *Chemtracts, Biochem. Mol. Biol. 2*, 379−389.
52. Fink, A. T. (1995) in *Methods in Molecular Biology, Vol. 40: Protein Stability and Folding: Theory and Practice* (Shirley, B. A., Ed.) Humana Press, Totowa, NJ.
53. Chan, H. S., and Dill, K. A. (1990) *Proc. Natl. Acad. Sci. U.S.A. 87*, 6388−6392.
54. Maier, C. S., Kim, O.-H., and Deinzer, M. L. (1997) *Anal. Biochem. 252*, 127−135.

BI981938W